



Priming and eruption of andesite magmas at Taranaki volcano recorded in plagioclase phenocrysts

Phil Shane¹ · Fidel Costa² · Shane Cronin¹ · Claudine Stirling³ · Malcolm Reid³

Received: 26 February 2023 / Accepted: 17 July 2023
© The Author(s) 2023

Abstract

Plagioclase phenocrysts in pre-historic andesites provide insight to the dynamics of magma formation and eruption at Taranaki volcano, New Zealand. The phenocryst population has a diversity of relic cores and a total in situ $^{87}\text{Sr}/^{86}\text{Sr}$ range of 0.70440–0.70486. Within-sample $^{87}\text{Sr}/^{86}\text{Sr}$ variations of 0.00018 to 0.00043 indicate that many phenocrysts are antecrysts and/or xenocrysts, derived from multiple crystal mush bodies. The Sr-isotopic differences in the phenocrysts of consecutive eruptions indicate that different magmas were tapped or formed on a centennial timescale. Most phenocrysts have multiple resorption/calcic regrowth zone(s) with elevated FeO* but invariant MgO zonation profiles. They likely record mafic melt inputs, and subsequent storage at elevated temperature caused re-equilibration of the Mg gradient. However, distinct rim types record different final pre/syn-eruptive magmatic conditions. Those in magmas erupted at 1030–1157 CE, 1290–1399 CE and 1780–1800 CE are characterised by resorption and calcic regrowth with sharp MgO and FeO* gradients. They record the entry of mafic melt into the system a few days or less before eruption based on Mg diffusion chronometry. In contrast, most phenocrysts erupted at 1755 CE, 1655 CE, and a few pre-1 ka events, have texturally uniform rims, compositionally consistent with closed-system crystallisation. This suggests alternating external and internal eruption triggers. Alternatively, the rate of magma reactivation via intrusion may dictate whether there was sufficient time for a mineralogical response to be recorded in part or all of the system. With respect to anticipating future eruptions, the plagioclase phenocrysts suggest multi-stage magma priming but rapid onset of the final trigger.

Keywords Eruption triggering · Antecryst · Plagioclase · Diffusion chronometry · New Zealand · Sr isotopes

Introduction

Geophysical and geochemical phenomena resulting from the rise and storage of magma and its trigger to eruption are of great interest when anticipating future eruptions at volcanoes (Pallister and McNutt 2015), especially for frequently active arc volcanoes. Instrumental monitoring and the petrology of the erupted magmas demonstrate that many

directly observed andesitic-dacitic eruptions were preceded by mass and heat transfer during the ascent of new mantle-derived magmas into older and shallow crustal reservoirs (e.g. Pallister et al. 1996; Murphy et al. 2000; Coombs et al. 2013). At volcanoes where eruptions have not been directly observed, retrospective criteria for determining conditions conducive to magma assembly and eruption must be inferred. In these situations, phenocrysts in erupted deposits are important archives of magmatism (e.g. Davidson et al. 2007; Ginibre et al. 2007; Ubide and Kamber 2018; Costa 2021). Such studies show that even small-to-medium-sized andesitic-dacitic magmas ($\sim 0.001\text{--}3\text{ km}^3$) may have been primed for years to decades from multiple intrusions prior to eruption (e.g. Costa and Chakraborty 2004; Metcalfe et al. 2021; Mangler et al. 2022), raising the question what is the final trigger that drives volcanoes to erupt? A variety of final triggers beyond the entry of new melt have been suggested including pressurisation from volatile exsolution induced by crystallisation (Tait et al. 1989; Cassidy et al. 2019);

Editorial responsibility: Y. Moussallam

✉ Phil Shane
pa.shane@auckland.ac.nz

- ¹ School of Environment, University of Auckland, Auckland 1142, New Zealand
- ² Institut de Physique du Globe de Paris, Université de Paris Cité, 75238 Paris Cedex 0, Paris, France
- ³ Department of Geology & Centre for Trace Element Analysis, University of Otago, Dunedin 9054, New Zealand

open-system volatile ‘flushing’ of the conduit from deeper degassing magmas (Caricchi et al. 2018); or depressurisation of the overburden via passive gas release during periods of quiescence (Girona et al. 2016). Long term decoupling of volatiles and melts during crustal migration is likely to result in reservoir instability (Christopher et al. 2015). Using phenocryst textures to distinguish between these processes and melt input is an ongoing challenge, and of significant importance because future pre-eruption unrest may differ depending on the mechanisms involved.

In this study, we examined plagioclase phenocrysts in deposits from several pre-historic eruptions of Taranaki volcano, New Zealand (Fig. 1), with the aims of (a) assessing the provenance of the crystal cargo and its lineage to the carrier magma; and (b) exploring the conditions that led to eruption. Plagioclase was the focus because the slow diffusion of major and many minor elements make it an excellent archive of magmatic processes. In crustal settings, plagioclase composition is mostly controlled by temperature (T), water pressure ($P_{\text{H}_2\text{O}}$) and melt (X) (Sisson and Grove 1993; Panjasawatwong et al. 1995), and it can potentially record the evolutionary pathway of the melts such as closed-system fractional crystallisation or open-system mixing (e.g., Singer et al. 1995; Ginibre et al. 2002; Smith et al. 2009). The high Sr contents of plagioclase allows in situ, sub-crystal-scale

analysis of $^{87}\text{Sr}/^{86}\text{Sr}$ that can record the crustal and/or mantle signature of the parental melt(s) and thus indicate the provenance of the phenocrysts (Davidson et al. 2007; Shane et al. 2019). Additionally, post-crystallisation elemental diffusion can give relative or absolute insight to the timescales of magma processes (Costa et al. 2003).

Of New Zealand’s dormant but recently active arc volcanoes, Taranaki volcano (Cronin et al. 2021) has received less attention from the perspective of magmatic modelling of eruption potential. This is partly the result of its isolated location in the western North Island (Fig. 1) away from the active volcanic front of the Taupo volcanic zone (Cole 1990), and because its last eruption occurred in 1790 CE (Platz et al. 2012; Lerner et al. 2019) and was not recorded in historical literature. Tephra records demonstrate that Taranaki volcano has been frequently active, and the current period of quiescence is anomalous (Damaschke et al. 2018). Furthermore, ash from previous eruptions has been widely dispersed including to major urban areas such as Auckland city (Molloy et al. 2009). So future eruptions are potentially a nationwide hazard. The petrogenesis of Taranaki magmas is well documented from whole rock analysis and mineralogy (Stewart et al. 1996; Price et al. 1999; Zernack et al. 2012; D’Mello et al. 2023), and such studies have focussed on determining the deep source of the melts. Less attention has been given to magma interactions and ascent in the crust recorded at crystal and sub-crystal scales (cf., Higgins 1996; D’Mello et al. 2021).

Here, we show the potential for plagioclase textures to record multi-stage intrusive priming of magma reservoirs and conditions just before eruption. However, we also show that the rate of magmatic reactivation may not provide sufficient time to induce a mineralogical response.

Geological background and samples

Taranaki volcano is an andesitic stratovolcano located ~400 km west of the Hikurangi Trench (Fig. 1) which is the southern extension of the Tonga-Kermadec subduction system. In northern New Zealand, the oceanic Pacific Plate obliquely subducts westward beneath the continental Australian Plate and is associated with the currently active arc volcanism of the Taupo volcanic zone (TVZ) (Cole 1990). Taranaki volcano is isolated some 140 km west of the volcanic front. The cause of the volcanism in space and time is uncertain (Cronin et al. 2021), but a Wadati–Benioff Zone dips sub-vertically at >200 km depth near Taranaki volcano (Reyners et al. 2006), and its magmas have geochemical features typical of arc volcanoes (Price et al. 1999). Based on seismicity, the thickness of brittle crust varies abruptly from ~35 km east of the volcano to ~25 km thick to the west but is only ~10 km thick immediately beneath the volcano

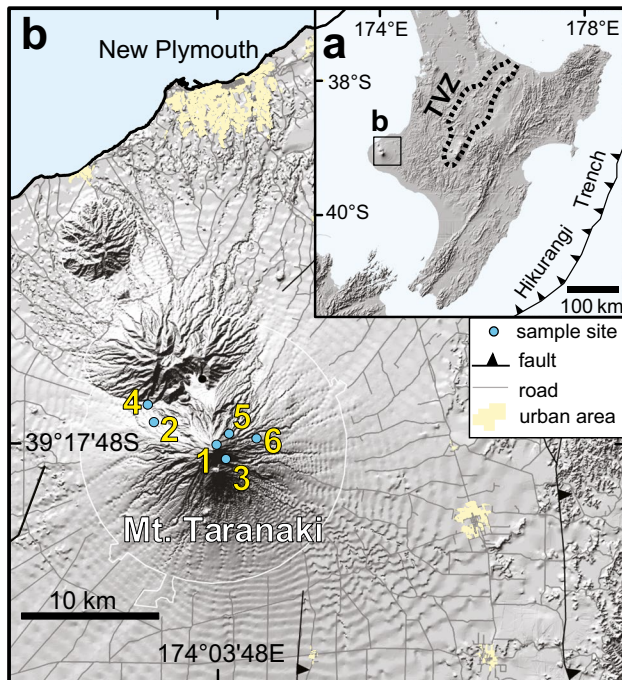


Fig. 1 **a** Map of North Island, New Zealand showing the location of Taranaki volcano and the Taupo volcanic zone (TVZ). **b** Map of Taranaki volcano showing the location of sample sites: 1 = Pyramid, Summit; 2 = Tahurangi, Newall; 3 = Burrell; 4 = Te Popo; 5 = Staircase and 6 = Warwicks Castle (see Table 1)

due to localised high heat flow (Sherburn and White 2006). Taranaki volcano is part of a chain of andesite volcanoes where activity commenced at ~1.7 Ma and the locus of volcanism migrated southeast to its current site (reviewed by Cronin et al. 2021). The central eruptive vent of the volcano has been active for ~14 ka and has an edifice of mostly lava flows of ~12 km³ in volume.

Taranaki lavas are porphyritic with phenocrysts, typically ~500 to 2000 µm in length, comprising 25–55 % of the rock (Stewart et al. 1996; Price et al. 1999). Abundant plagioclase and subordinate clinopyroxene and/or amphibole are ubiquitous in the phenocryst assemblage. Other subordinate phases are Fe-Ti oxides, olivine and rarely orthopyroxene. The groundmass is micro-crystalline comprising of the same components, particularly plagioclase and clinopyroxene, and interstitial glass. The rocks are texturally homogeneous, lacking mafic enclaves or mingled groundmass. Most rocks are high-K, low-Si andesites, subordinate basalts and dacites also occur. The younger deposits are characterised by higher K₂O, Rb, Ba and Zr contents (Price et al. 1999). All the rocks display relative enrichments in large ion lithophile elements (LILE) and depletions in high field strength elements (HFSE) typical of subduction zone magmas.

Samples selected for study are from the main lava flow suites (pre-1 ka) that form the current edifice, and pyroclastic deposits from the post-1 ka series of eruptions (Table 1). Stewart et al. (1996) divided edifice lavas into groups. The Warwick's Castle Group are the oldest flows on cone (~3 to 8 ka) and occur as distinctive ponded lava flows with columnar jointing, up to 100 m thick. They are overlain by the Staircase Group (0.7 to 2 ka) which are thinner (10–20 m thick) valley-filling lavas. The Summit Group are the youngest lava flows (<0.7–1 ka) and form the summit crater and fill radial valleys. They comprise of thin flows and coulees.

We collected a sample from each of these lava groups (Table 1). Post-1 ka (~1130 to 1800 CE) proximal deposits are referred to as the Maero Formation (Platz et al. 2012; Lerner et al. 2019). It comprises of deposits from at least 11 eruptive events separated by paleosols. Repose periods vary from within uncertainty of radiocarbon dating to about 200 years. Each involved dome extrusion at the summit crater, and subsequent collapse producing block and ash flow deposits (~0.01–0.03 km³) with associated sub-Plinian and/or other fall deposits (mostly ~0.5–1.0 km³). The youngest eruption was a dome extrusion at 1780–1800 CE (Pyramid dome). Samples representing discrete eruptions were selected for study and include the Te Popo, Newall, Burrell, Taurangi and Pyramid eruptions (Table 1).

Methods

Analytical methods

Zonation patterns in plagioclase phenocrysts were investigated via backscatter electron (BSE) imaging of polished rock thin sections. Quantitative spot analyses were performed using a JEOL field emission electron probe (8530F Hyperprobe) at the University of Auckland. Plagioclase compositions were determined using a 15-kV acceleration voltage, 20-nA current, and a beam size of 3 µm. Replicate analyses on plagioclase standard NMNH 115900 were used to give an indication of precision and accuracy. Peak counting times were 30 s for the elements Si, Al, Ca, Na and K and they have estimated 1 σ uncertainties of ± 1%. For Mg and Fe, extended counting times (90 s) and the use of large TAP and LIF spectrometer crystals gave estimated uncertainties of ~ ± 6 and ± 3%, and detection limits of ~17

Table 1 Taranaki rock samples used in this study

| Eruption episode (sample no.) | Date | WR SiO ₂ (wt %) | WR MgO (wt %) | Deposit | Lat/Long | Ref |
|--------------------------------|--------------|----------------------------|---------------|-----------|-------------------------|-----|
| Maero pyroclastic group | | | | | | |
| Pyramid (67411) | 1780–1800 CE | 58.12 | 2.86 | Lava dome | 39°17'43"S, 174°03'49"E | 1 |
| Taurangi (68171, M5A) | 1755 CE | 58.00 | 3.16 | PDC clast | 39°16'44"S, 174°00'37"E | 2 |
| Burrell (57223) | 1655 CE | 57.87 | 2.99 | PDC clast | 39°18'19"S, 174°03'56"E | 3 |
| Newall (68150, M1H) | 1290–1399 CE | 59.97 | 2.60 | PDC clast | 39°16'44"S, 174°00'37"E | 2 |
| Te Popo (68194, P1A) | 1030–1157 CE | 60.02 | 2.61 | PDC clast | 39°16'07"S, 174°00'48"E | 2 |
| Edifice lava flows | | | | | | |
| Summit (T89-15) | 0.7–1 ka | 55.02 | 3.58 | Lava flow | 39°17'46"S, 147°03'55"E | 4 |
| Staircase (T89-24) | 0.7–2 ka | 54.66 | 3.87 | Lava flow | 39°17'21"S, 174°04'41"E | 4 |
| Warwick's Castle (T89-21) | 3–8 ka | 55.98 | 3.04 | Lava flow | 39°17'46"S, 174°05'04"E | 4 |

Ref = References refer to the original sample collection and data. 1 = Zorn (2017), 2 = Lerner et al. (2019), 3 = Platz et al. (2012), 4 = Price et al. (1999)

WR whole rock (normalised water free)

and ~55 ppm, respectively. The elements Ti, Mn and Ba were also detected, but are of low abundance in the standard and samples and were not used. A full dataset is in Online Resource 1.

The method for determining in situ $^{87}\text{Sr}/^{86}\text{Sr}$ in plagioclase was the same as that described in Shane et al. (2019) and Cocker et al. (2021). Briefly, the $^{87}\text{Sr}/^{86}\text{Sr}$ values were measured at the Centre for Trace Element Analysis, University of Otago using a Nu Plasma-HR multi-collector inductively coupled plasma mass spectrometer (MC-ICPMS), coupled to a RESOLUTION excimer laser ablation system. Typical 2σ uncertainties were ± 0.00003 to 0.00007 and represent instrumental and external uncertainties calculated from the reproducibility of repeat measurements of in-house standards and reference materials. BSE images of the phenocrysts were used to select sites for laser ablation (~100 μm wide and 400–600 μm long). Where possible the ablation zones were oriented parallel to crystal growth bands to avoid crossing major compositional domains. It is likely that unobserved crystal domain boundaries were encountered in the ablation pits where growth zones were narrow. A total of 121 $^{87}\text{Sr}/^{86}\text{Sr}$ analyses on 68 phenocrysts were obtained. A full dataset is in Online Resource 1.

Diffusion chronometry

For rim overgrowths of plagioclase phenocrysts with sharp compositional gradients, we modelled their duration at magmatic temperatures from the diffusion of Mg. Initial Mg profiles can be inferred from the X_{An} (mol fraction of anorthite) patterns because of the slow rate of coupled NaSi–CaAl exchange compared to Mg diffusion at the same temperature (Cherniak 2010) and the assumption that a high Ca/Na melt also had a high Mg content (as observed for rim growths in this study). A numerical (finite difference) algorithm computed the change in plagioclase composition over time. The rim of the phenocryst was assumed to be an open system with the melt. We used the diffusion coefficient of Van Orman et al. (2014). To model the diffusive equilibration of Mg in plagioclase we used the partitioning relations (equations 2 to 5) of Mutch et al. (2022) which need to be incorporated into the diffusion equation 7 of Costa et al. (2003). However, it is unclear how the different terms of equations 2 to 5 can be partially differentiated in equation 7 of Costa et al. (2003) to obtain a general equation that could be applied to any crystal for modelling the diffusive re-equilibration of Mg. Thus, we instead first calculated the partition coefficient of Mg (K_{Mg}) with Mutch et al. (2022) equations for each crystal. Then we did a linear fit to the K_{Mg} and An data using the simple relation $RT\ln K_{\text{Mg}} = AX_{\text{An}} + B$ for each crystal (see Online Resource 1), where T is temperature (K), and R is the universal gas constant ($\text{kJ mol}^{-1}\text{K}^{-1}$). Thus, we obtained the values of the parameter A , which can

then be directly incorporated into equation 7 of Costa et al. (2003). We found that most crystals show good linear correlations between X_{An} and $RT\ln K_{\text{Mg}}$ (R2 values between 0.91 and 0.97), and they all give similar values of the A and B parameters. The poorest fit for these relations was R2 of 0.78 (crystal 6711A-03) but the slope (values of A) was still coherent for all the data. Note that either the fits to the data or the timescales we calculated using the K_{Mg} of Bindeman et al. (1998) or Mutch et al. (2022) are within error. However, this is not a general finding (see discussion in Mutch et al. 2022), but we believe it occurs in our samples as there is very limited diffusion and thus the effects of the selected K_{Mg} on the timescales are minimal.

Plagioclase textures and compositions

Phenocryst interiors

The plagioclase phenocrysts display considerable textural and compositional (~An₃₀₋₉₀) diversity and all record episodes of partial resorption and regrowth. Most comprise of a subhedral or anhedral relic core surrounded by an inner ‘mantle’ and outer ‘rim’ zone where the textural patterns and compositions change abruptly at major resorption surfaces (Fig. 2). In addition, minor resorption surfaces associated with more subtle zonation may occur within these broader zones. All phenocrysts have an outermost rim overgrowth that is oscillatory zoned (see below).

Based on interior characteristics, phenocrysts were divided into four major types (Types 1–4) (Fig. 2). Type 1 phenocrysts are the most common and variously represent ~40–80% of the plagioclase phenocrysts in the samples, except for Staircase lava (11%) (Table 2). They are characterised by highly resorbed relic calcic cores (~An₇₀₋₈₀) that display diffuse patchy zoning or lacks zonation (Fig. 2a, b). The cores have been irregularly and extensively replaced by more sodic plagioclase (~An₅₀₋₆₀). The mantle zones surrounding the cores have similar compositions (~An₅₀₋₆₀) and comprise of one to three normal-zoned growth cycles. Commonly, the mantle zones display a patchy texture due to an episode of sodic replacement that in some cases obscures the original texture. In many phenocrysts, the outer part of the mantle zones has been resorbed and overgrown by more calcic plagioclase (~An₆₀₋₇₀). This event has produced a sieved-like texture where channels of calcic plagioclase and melt penetrate towards the interior, and crystal and glass micro-inclusions are abundant (Fig. 2b).

Type 2 phenocrysts variously represent 18–45% of the phenocrysts in the samples but are rare in sample Warwick’s Castle lava (Table 2). They are characterised by oscillatory zoning throughout their interiors. Most lack of a relic core zone (Fig. 2c, d), or more rarely, have a small anhedral relic

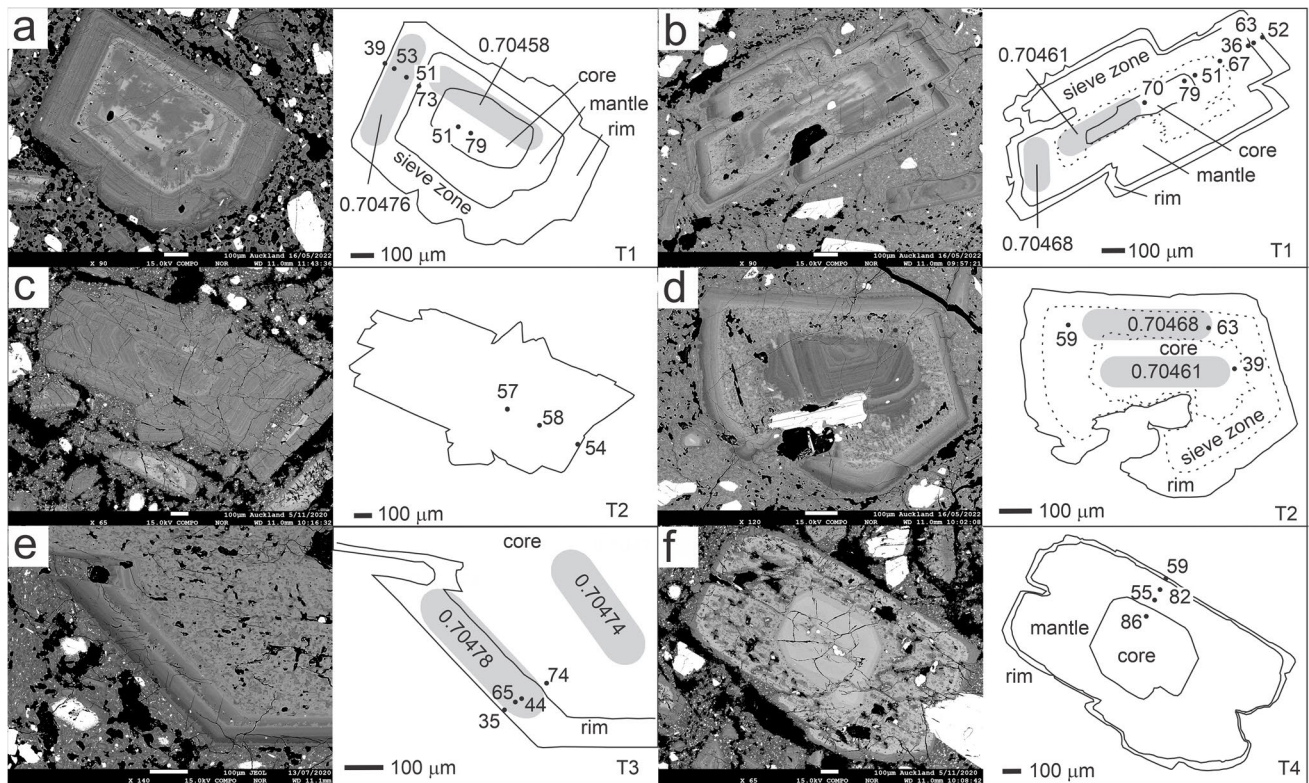


Fig. 2 BSE images of major phenocryst types. **a, b** Type 1 phenocrysts comprising of calcic resorbed cores and mantle overgrowths, both with patchy texture from sodic replacement, and oscillatory zoned rims (crystals 57223A-08; P1A-A01). Calcic sieve texture is seen in (b). **c, d** Oscillatory-zoned Type 2 phenocrysts lacking a relic core. Calcic sieve texture mantle is seen in (d) (crystals T89-15A-10;

P1A-A04). **e** Type 3 phenocryst showing a ‘wormy’ texture resulting from extensive calcic replacement in the interior (crystal 67411A-06). **f** Type 4 phenocryst with a highly calcic euhedral relic core (crystal T89-15A-06). In sketches, two-digit numbers refer to An contents at spots. Five-digit numbers and grey shaded areas represent ⁸⁷Sr/⁸⁶Sr values and their analytical zone

Table 2 Modal abundance of plagioclase phenocryst and rim types

| Sample | Phenocryst type (%) | | | | Rim type (%) | | |
|-----------|---------------------|----|----|----|--------------|----|----|
| | T1 | T2 | T3 | T4 | R1 | R2 | R3 |
| Pyramid | 44 | 42 | 11 | 3 | 0 | 10 | 90 |
| Tahurangi | 63 | 26 | 5 | 5 | 53 | 47 | 0 |
| Burrell | 40 | 24 | 20 | 16 | 91 | 9 | 0 |
| Newall | 74 | 26 | 0 | 0 | 14 | 0 | 86 |
| Te Popo | 45 | 45 | 5 | 5 | 0 | 21 | 79 |
| Summit | 55 | 18 | 27 | 0 | 96 | 4 | 0 |
| Staircase | 11 | 36 | 39 | 14 | 100 | 0 | 0 |
| Warwicks | 83 | 0 | 4 | 13 | 22 | 78 | 0 |

Based on 70–100 of the largest phenocrysts in thin section

core. Broadly, they have a compositional range of ~An₄₀₋₆₅ (mostly An₅₅₋₆₅). All oscillatory cycles are normal zoned and start with an irregular resorption surface followed by calcic regrowth. In the interior of the phenocrysts, cycles are typically up to 40–50 μm in wavelength and involve amplitudes up to An₁₀. Typically, the cycles are progressively shorter in wavelength (typically 10–20 μm) and involve smaller amplitudes (up to ~An₅) towards the rim. Many Type 2

phenocrysts record one or two major resorption events followed by calcic (~An₇₀₋₈₀) regrowth forming a sieve-like textured zone (Fig. 2d), like those described for Type 1 phenocrysts.

Type 3 phenocrysts are a subordinate group that are found in most samples but are common in Staircase lava (39 %) (Table 2). They have a broad uniform-appearing interior with a fine sieve-like texture (~An₇₀₋₈₀) (Fig. 2e).

The interior zones have ‘wormy’ appearance where calcic plagioclase forms a network of fine channels comprising of melt and recrystallised plagioclase around relic sodic patches (1–10 µm wide). Voids and micro-inclusions are common. These interiors are commonly surrounded by a calcic overgrowth that ‘seals’ the channels.

Type 4 phenocrysts are another subordinate group found in most samples (Table 2). They are distinguished by euhedral-subhedral, highly calcic ($\sim\text{An}_{80-93}$) cores (Fig. 2f). These cores lack zoning or have diffuse patchy zoning, and many have a euhedral outer growth(s) of less calcic plagioclase ($\sim\text{An}_{70}$). The remainder of the phenocryst variously consist of mantle and rim overgrowths like those described for Type 1 and 2 phenocrysts.

The abundance of MgO and FeO* (total Fe) in the phenocrysts are in the range ~ 0.01 – 0.07 wt % and 0.2 – 0.8 wt %, respectively. Their zonation patterns do not uniquely correlate with An content (Fig. 3) and therefore, phenocryst type. In phenocryst cores and mantles, there is a weak positive or negative An-MgO correlation for more sodic and calcic compositions, respectively, but there is considerable scatter (Fig. 4). The rim zones in the Pyramid, Newall and Te Popo samples are enriched in MgO (Fig. 4a, d, e) and FeO* (Fig. 5a, d, e). Overall, FeO* and An contents show a positive correlation in the mantle zones, but not core zones (Fig. 5).

Phenocryst rims

The rims were defined as zones with distinct textural characteristics that formed following the last major resorption event, and three growth patterns were observed (R1–3). Rim type 1 (R1) are wide (~ 100 – 400 µm), uniformly oscillatory-zoned, and lack major dissolution/regrowth disturbances (Fig. 6a). They represent ~ 50 – 100 % of phenocryst rims in the Tahurangi, Burrell, Summit, and Staircase samples, but are absent in the Pyramid and Te Popo samples (Table 2). The oscillatory cycles are ~ 5 – 10 µm wide and normal-zoned. They are bounded by minor sharp and irregular resorption surfaces and start with calcic regrowth. Intra-cycle compositional variation is $< \text{An}_{10}$ and not accompanied by regular patterns in FeO* or MgO content. In some cases, finer diffuse cycles (1–2 µm wide) involving small compositional changes ($\sim \text{An}_{1-2}$) occur within the wider cycles. In many phenocrysts, the cyclic patterns are superimposed on a secular rim-ward decline in An, MgO and FeO* contents. Type 2 rims (R2) comprise of a prominent dissolution surface and a normal-zoned regrowth that is ~ 20 – 50 µm wide (Fig. 6b). They are common in the Tahurangi and Warwicks Castle samples (Table 2). The regrowth begins with a sharp and irregular resorption surface where calcic plagioclase has regrown on more sodic plagioclase. The compositional changes across the resorption surface are up to $\sim \text{An}_{20}$. In

most phenocrysts, FeO* and An contents are positively correlated and MgO is invariant. Diffuse, ~ 1 – 2 µm-wide, oscillatory cycles are superimposed on some of the regrowth zones and involve compositional variations of $\sim \text{An}_{1-2}$.

In addition to the wide rim zones described above, some phenocrysts have a thin outermost rim (~ 10 – 15 µm wide) characterised by elevated An, FeO* and MgO contents (Fig. 6c). These are referred to as Rim type 3 (R3) and are ubiquitous in the Pyramid, Newall and Te Popo samples (~ 80 – 90 % of phenocryst rims) but are absent in the other samples (Table 2). R3 rims comprise of a sharp and irregular resorption surface followed by a calcic ($\sim \text{An}_{60-70}$) regrowth zone that is normal-zoned trending down to $\sim \text{An}_{50}$ (Fig. 6c). Sharp compositional gradients across the resorption surface involve variations of $\sim \text{An}_{20-30}$; FeO* ~ 0.20 wt % and MgO ~ 0.04 – 0.05 wt %. Some comprise of two or more cycles of dissolution and normal-zoned regrowth. The final regrowth cycle is the most calcic and magnesian. Other rare examples are associated with a thin band of sieve-like texture comprising of a channel network of high-An growth. Most of the outermost rims display diffuse oscillatory-cycles with widths of < 1 – 2 µm involving minor compositional contrasts of $\sim \text{An}_{1-2}$.

Plagioclase Sr isotopes

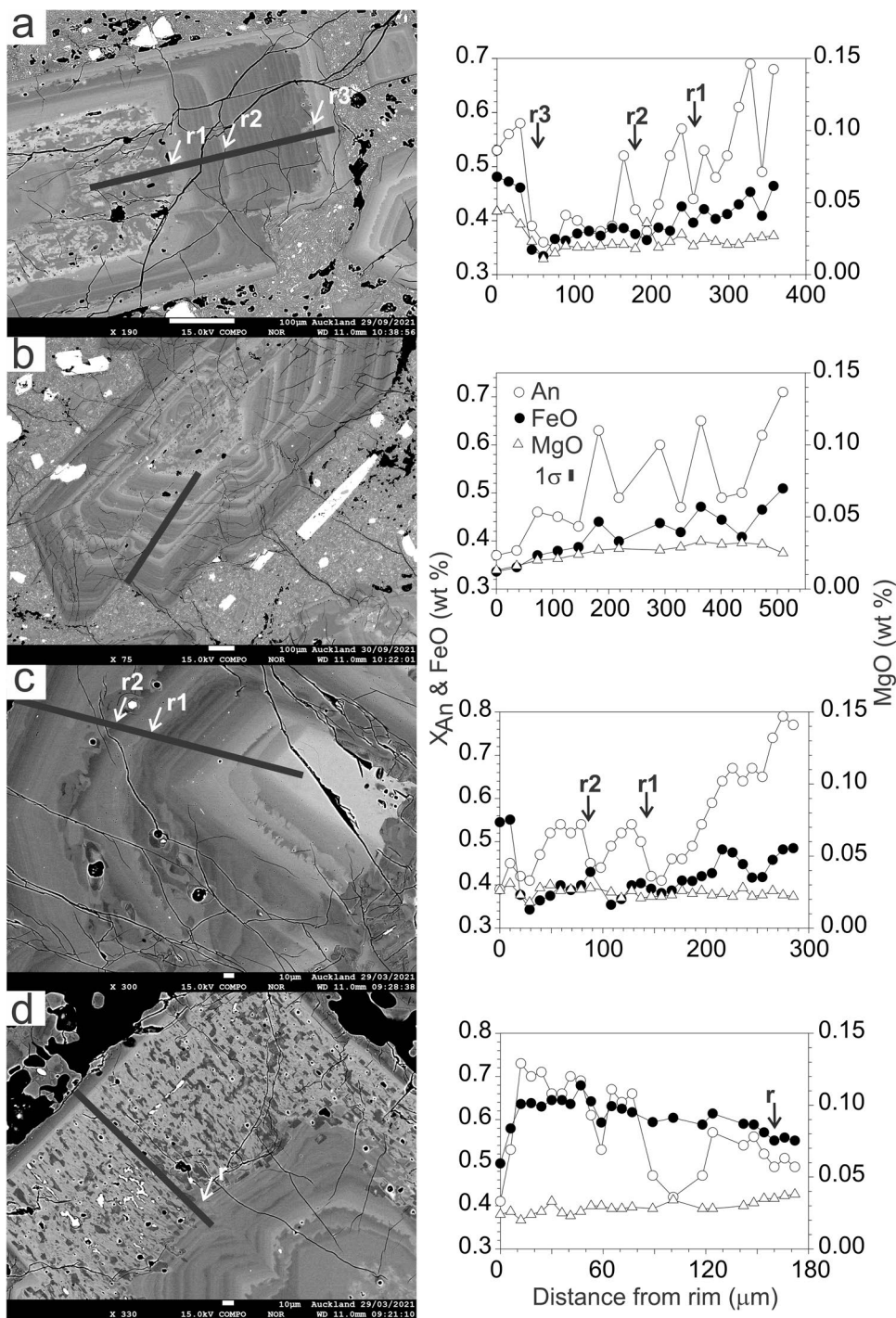
In situ analysis of 68 plagioclase phenocrysts (Table 3; Fig. 7) produced $^{87}\text{Sr}/^{86}\text{Sr}$ values of 0.70440 – 0.70486 ($n = 121$). This isotopic range (0.00046) is greater than the typical average analytical uncertainty (± 0.00005 to 0.00007). Inter-crystal ranges within the various samples are 0.00018 to 0.00043 , with the greatest homogeneity in Tahurangi and Warwick’s Castle samples and least in Newall sample (Table 3). Based on core and rim analyses, nearly all intra-crystal isotopic variability is within or close to analytical uncertainty. An exception is one crystal in the Newall sample with a core-rim difference of 0.00029 (± 0.00006). For the Pyramid sample, high Sr contents in the plagioclase inferred from ^{88}Sr V measurements and greater ablation volumes allowed greater $^{87}\text{Sr}/^{86}\text{Sr}$ precision (± 0.00003). This revealed intra-crystal variability of up to 0.00011 .

Discussion

Melt compositions from plagioclase Ca/Na

In the absence of glassy rocks, inferences of the melt compositions can be made from phenocryst compositions. Previous studies have demonstrated the potential of Ca/Na plagioclase-melt partitioning to investigate the equilibrium melt composition for neighbouring TVZ volcanoes (Shane et al. 2019; Cocker et al. 2021, 2022). Since the diffusion rate of

Fig. 3 BSE images and compositions of phenocrysts selected to show typical relationships between texture and chemistry. **a** Type 1 phenocryst showing two major resorption surfaces not associated with change in Fe or Mg contents (r1, r2), and the one that is (r3). Crystal M1H-A06. **b** Type 2 phenocryst with oscillatory cycle texture and rim-ward declining Fe and Mg contents. Crystal P1A-A16. **c** Type 4 phenocryst with two major resorption surfaces marked that are not associated with change in Fe or Mg contents (r1, r2). Crystal 57223A-06. **d** Type 1 phenocryst with a sieve-textured mantle zone that has elevated Fe but invariant Mg contents. Crystal 57223A-03. Black line is analytical profile. Scale is shown on graph axis. Analytical uncertainty equal to symbol size except where shown



NaSi-CaAl coupled exchange is slow (Grove et al. 1984), the original zoning patterns are likely to be preserved. In the crustal conditions expected beneath Taranaki volcano (<10 kbar, <38 km), magmatic water content (P_{H_2O}) would have the dominant control on the Ca/Na of plagioclase, while temperature and melt composition are subordinate (Sisson and Grove 1993; Panjasawatwong et al. 1995). Higher magmatic water contents and temperature, and/or calcic melts

will nucleate more calcic plagioclase. D’Mello et al. (2023) estimated water contents for Taranaki magmas of ~1–3 wt % based on plagioclase-melt equilibria. This equates to $K_{Ca/Na} = \sim 1$ based on several experimental andesitic/basaltic datasets (see Martel et al. 2006). A caveat is that conditions may have changed during magma evolution. The presence of amphibole (Stewart et al. 1996) which is typically stable in andesites at higher water contents (e.g., ~5–6 wt %, Martel

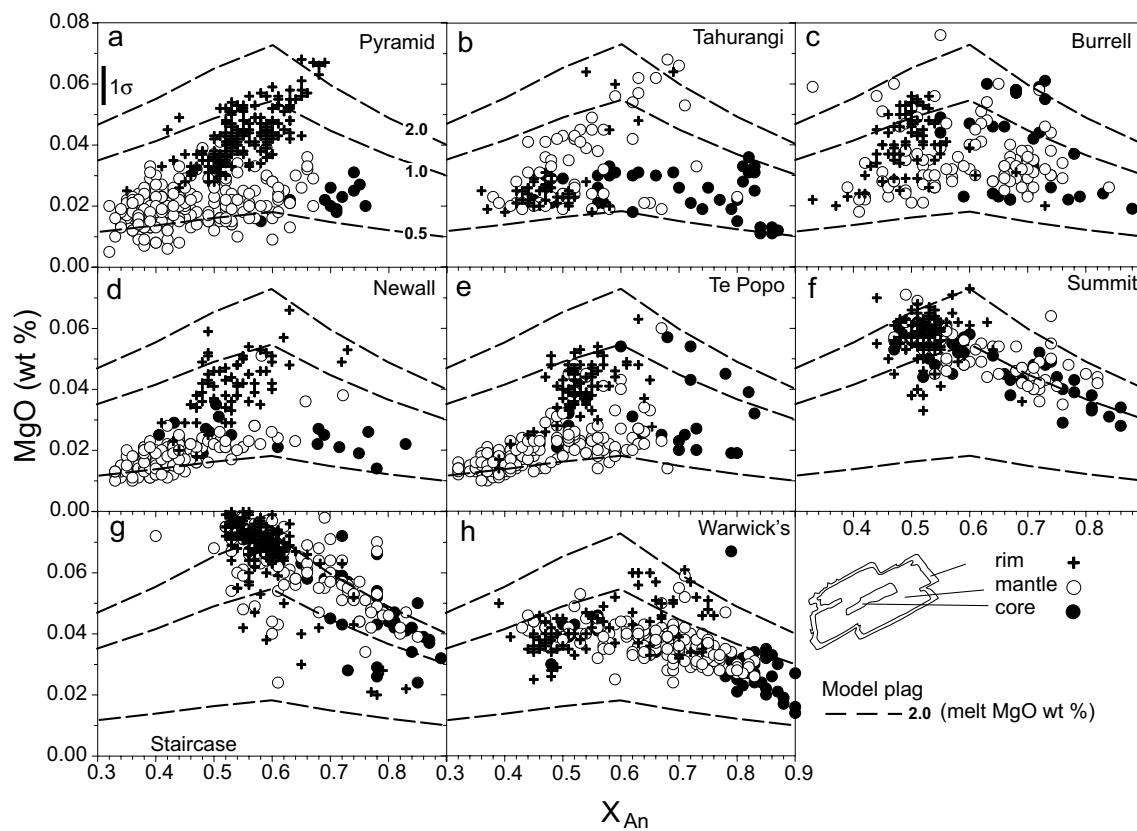


Fig. 4 Composition (An-MgO) of plagioclase phenocrysts in the samples examined separated into core, mantle, and rim zones. **a–e** Post-1 ka samples. **f–h** Pre-1 ka samples. Curves represent the mod-

elled equilibrium composition of plagioclase for melts of varying MgO content (wt %) shown as numbers (see text). Analytical uncertainty equal to symbol size except where shown

et al. 1999), would equate to $K_{Ca/Na} = \sim 3$ (Fig. 8). However, there is significant textural and elemental evidence for disequilibrium in the mineral assemblage, and the absence of unreacted amphibole microlites in the groundmass indicates this phase may be non-cognate (D’Mello et al. 2023). Dacitic glass and andesitic whole rocks erupted post-8 ka from Taranaki volcano (Price et al. 1999; Platz et al. 2007; Damaschke et al. 2017; Lerner et al. 2019) provide a comparative basis for $K_{Ca/Na}$ modelling (Fig. 8) but may not be representative of liquids. In particular, the rocks contain abundant antecrysts and xenocrysts.

Assuming $K_{Ca/Na} = \sim 1$, the most calcic plagioclase ($Ca/Na > 5$; $>An_{83}$) would be in equilibrium with a melt of $Ca/Na > 5$, significantly greater than that of erupted compositions (Fig. 8). Such plagioclase compositions include the euhedral relic cores of Type 4. Plagioclase compositions ($\sim An_{60-80}$; $\sim Ca/Na$ 2–4) in the core zones of the most common phenocrysts (Types 1 and 2) would also be in equilibrium with a melt more calcic (and mafic?) than that of the erupted andesites (Fig. 8). The less calcic compositions of this range ($\sim An_{60}$) would require melts on the mafic end of the erupted range, like Fanthams Peak and Warwick’s Castle lavas. The most common rim compositions (Ca/Na

~ 1.2 ; $\sim An_{50}$) and common sodic replacement domains in the mantle zones ($Ca/Na < 0.75$; $< An_{40}$) would be in equilibrium with melts like that of erupted andesite rocks and dacite glass. In contrast, the calcic parts ($\sim An_{60-70}$) of the reverse zoned R3-type rims required an andesite/basalt melt.

Magmatic processes from MgO and FeO* in plagioclase

The minor elements Mg and Fe in plagioclase provide insight to the magmatic processes that operated during phenocryst growth and re-equilibration, although there are uncertainties associated with their crystal-melt partitioning behaviours. For Mg in plagioclase, the melt composition is thought to be the main control because An content, temperature and pressure exert a subordinate influence (Bindeman et al. 1998; Mutch et al. 2022). Some empirical studies suggest an Arrhenius-like relationship of decreasing crystal-melt partitioning coefficient (K_{Mg}) with increasing X_{An} (Bindeman et al. 1998). However, a recent data compilation and reanalysis of the effects of crystal-structural control on partitioning by Mutch et al. (2022) shows that the $K_{Mg}-X_{An}$ correlation changes from positive to negative

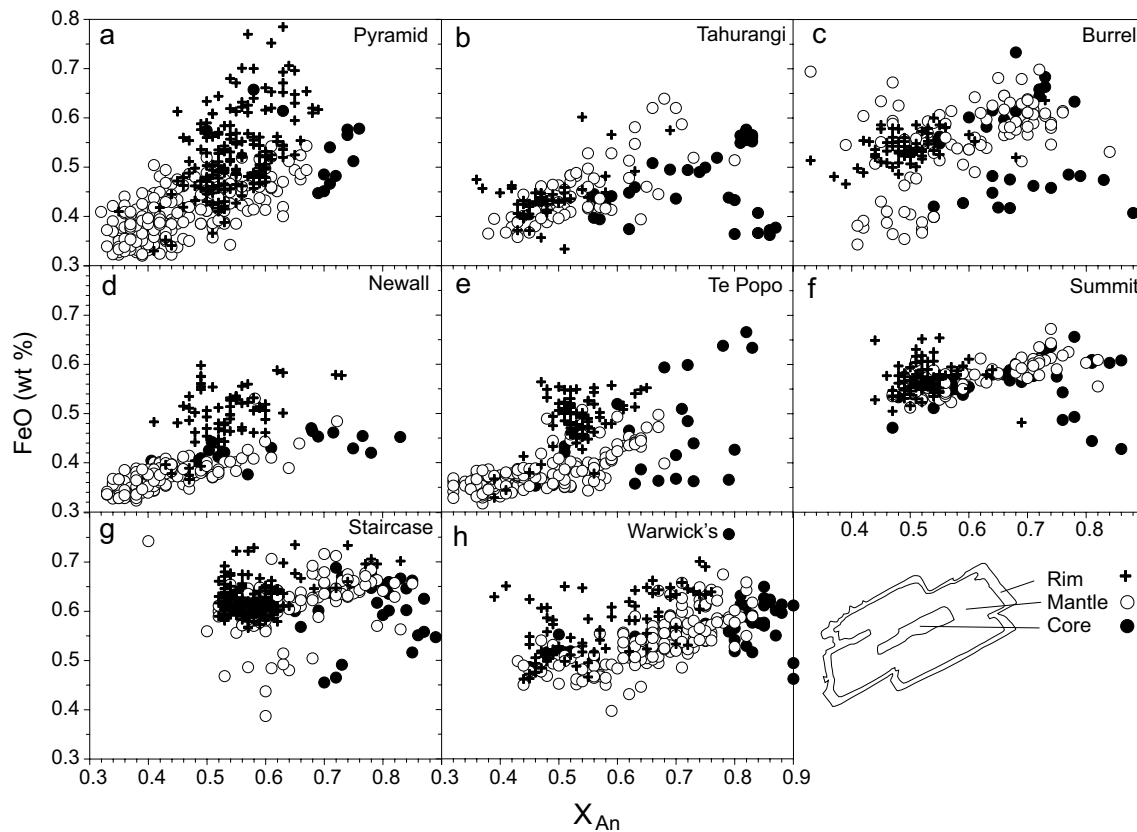


Fig. 5 Composition (An-FeO*) of plagioclase phenocrysts in the samples examined separated into core, mantle, and rim zones. **a–e** Post-1 ka samples. **f–h** Pre-1 ka samples. Analytical uncertainty equal to symbol size.

at $\sim\text{An}_{60}$, likely caused by Mg occupying different crystal lattice sites depending on Al in the structure. Their data also indicates K_{Mg} increases in more silicic melts. However, the Mg in plagioclase is strongly controlled by the melt composition regardless of the K_{Mg} assumed (Fig. 8 of Mutch et al. 2022). In a closed-system, fractional crystallisation of minerals found in Taranaki magmas (plagioclase, clinopyroxene, amphibole, and Fe-Ti oxides) would deplete the melt in Ca, Fe and Mg and result in progressively more sodic and less magnesian plagioclase. Conversely, open-system magma recharge would reverse the trend and produce more calcic/magnesian plagioclase. If the phenocryst is subsequently stored at magmatic temperatures for days to years, various degrees of post-crystallisation diffusion can redistribute Mg across domain boundaries towards an equilibrium composition (Costa et al. 2003). Some insight is provided by comparing zonation patterns of rapid (Mg) versus slow (Ca-Na) diffusing elements. The MgO content of plagioclase was modelled using the K_{Mg} of Mutch et al. (2022), assuming an ‘andesitic’ melt content of 60 wt % SiO_2 , and a temperature of 950 °C from mineral equilibrium data (Stewart et al. 1996; D’Mello et al. 2021). An increase of 50 °C increases the estimated MgO content of the equilibrium plagioclase

by $\sim 10\text{--}20\%$. The modelled plagioclase composition would represent equilibration at constant conditions in a melt of specified MgO content.

As expected, the chosen melt composition has the greatest control on the calculated Mg in the crystal and the scatter observed in the phenocrysts indicates formation in a range of melts and/or temperatures (Fig. 4). In pre-1 ka samples, the more calcic ($>\text{An}_{60}$) zones of phenocrysts form a negative An-MgO trend (Fig. 4f–h), consistent with diffusive re-distribution of Mg as modelled by Mutch et al. (2022). Re-equilibration of Mg in the core and mantle zones would be expected if the late-stage regime that caused the dissolution and regrowth of the rim zone was prolonged.

In post-1 ka samples, mantle zones show a weak positive An-MgO correlation (Fig. 4a, d, e), or are compositionally variable like the core zones (Fig. 4b, c), and there is no inflexion at $\sim\text{An}_{50-60}$ as predicted by the Mutch et al. (2022) model. More strikingly, the Mg-rich rim zones (R3 type) form steep positive An-MgO trends that cut across model curves indicating a change in melt composition (Fig. 4a, d, e). This is consistent with their textures that suggest major environmental changes in the magma during growth and incomplete re-equilibration of Mg. Specifically, rim-ward

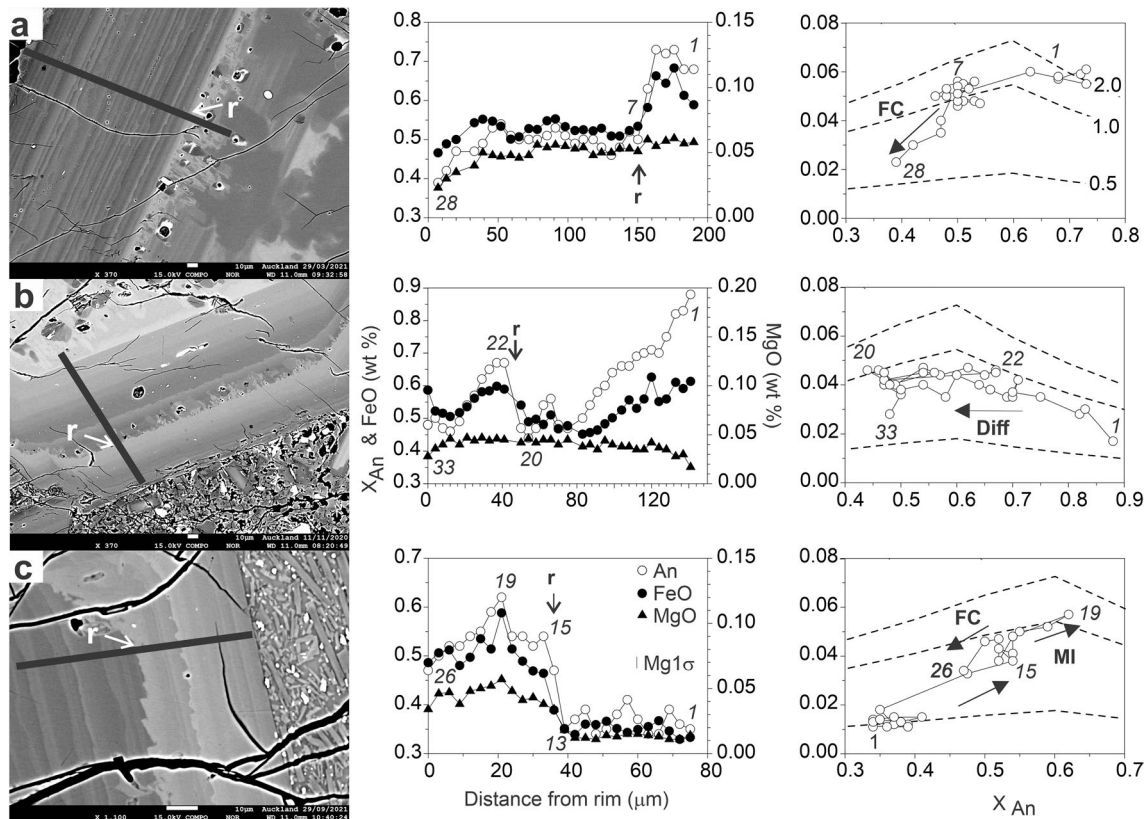


Fig. 6 BSE images and compositions of the three phenocryst rim types. The zones are defined by the final major resorption surface (*r*). **a** Type 1 oscillatory-zoned rim that lacks major dissolution/regrowth events (57223A-08). **b** Type 2 rim showing an episode of normal-zoned regrowth following a major resorption event (T89-21A-06). **c** Type 3 rim that comprises of a thin outermost rim with high An, Fe and Mg contents overgrown on a resorption surface. This example shows two cycles of growth (MIH-A06). Analytical profiles are

marked by a black line. Scale is on graph x-axis. Numbers (*italic*) in graphs represent sequential analytical position. Dashed curves on An-Mg plots represent the modelled equilibrium composition of plagioclase for melts of varying MgO content (wt %) shown as numbers (top panel). FC, fractional crystallisation; MI, mafic influx; Diff, diffusion. Analytical uncertainties are equal to symbol size except where indicated

Table 3 In situ $^{87}\text{Sr}/^{86}\text{Sr}$ values for Taranaki plagioclase

| Sample | Inter-crystal ^a | Δ^b | Intra-crystal ^a | Δ^b | 2σ |
|-----------|----------------------------|------------|----------------------------|------------|-----------|
| Pyramid | 0.70462–0.70485 | 0.00023 | 0.70467–0.70478 | 0.00011 | 0.00003 |
| Tahurangi | 0.70463–0.70482 | 0.00019 | 0.70463–0.70475 | 0.00012 | 0.00006 |
| Burrell | 0.70451–0.70482 | 0.00031 | 0.70452–0.70469 | 0.00017 | 0.00005 |
| Newall | 0.70443–0.70486 | 0.00043 | 0.70443–0.70472 | 0.00029 | 0.00006 |
| Te Popo | 0.70453–0.70477 | 0.00024 | 0.70453–0.70472 | 0.00019 | 0.00007 |
| Staircase | 0.70440–0.70471 | 0.00031 | 0.70454–0.70466 | 0.00012 | 0.00007 |
| Warwicks | 0.70453–0.70471 | 0.00018 | 0.70462–0.70470 | 0.00008 | 0.00007 |

2σ = uncertainty

^aRange of ratios from in situ spot analysis

^bDifference in range

reversals to higher An, FeO* and MgO contents occur in step-like patterns across one or two prominent resorption/regrowth surfaces (R3 rims, Fig. 6c). This could record a change from a low-Mg (~0.5 wt %) to a higher MgO (~2 wt %) melt (e.g., Fig. 6c). Crystal rims recording similar

processes have been observed in andesites worldwide and are attributed to the entry of a more mafic and hotter magma shortly before eruption (e.g. Murphy et al. 2000; Kent et al. 2010; Shane et al. 2019; Didonna et al. 2022). Following a crystal resorption event and calcic/magnesian regrowth, the

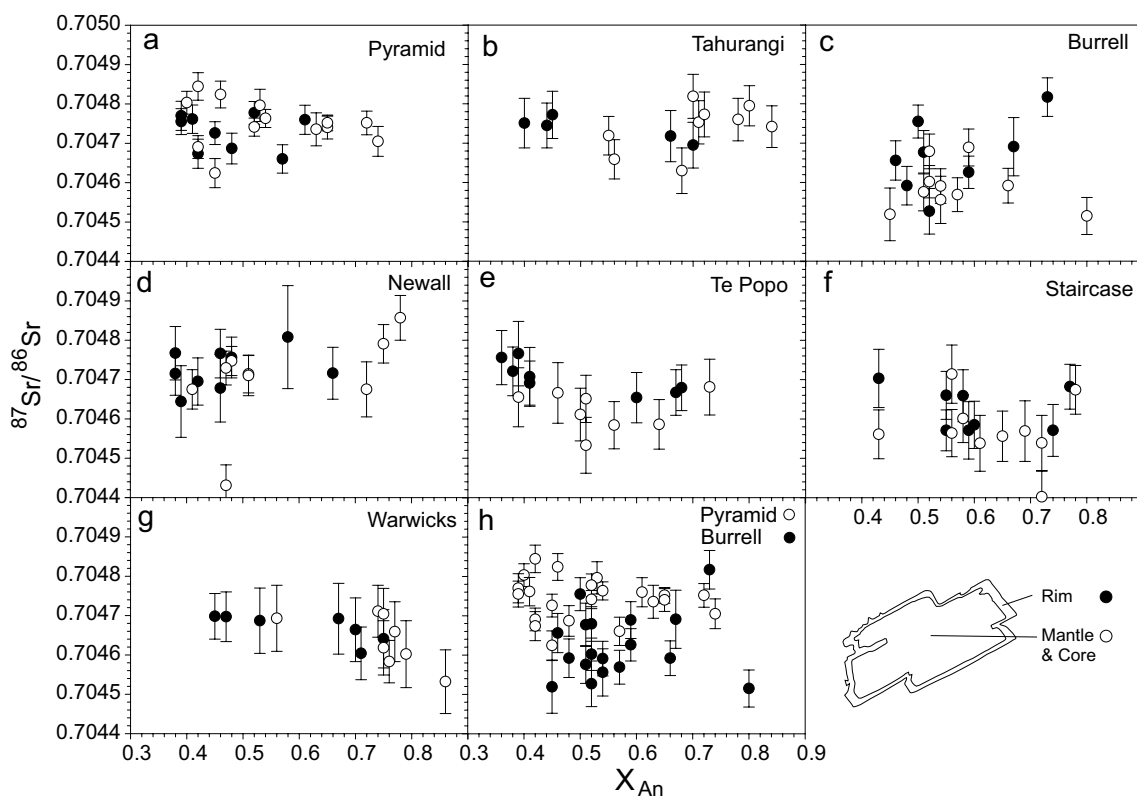
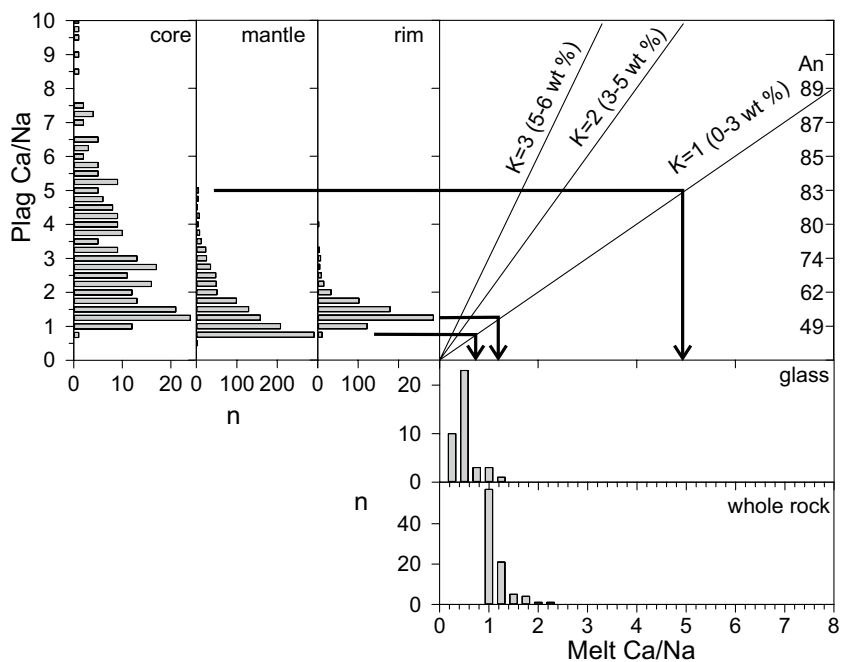


Fig. 7 The relationship between the composition of the plagioclase intra-crystal domain (An content) and its $^{87}\text{Sr}/^{86}\text{Sr}$ (error bar = uncertainty). **a–e** Post-1 ka samples. **f, g** Pre-1 ka samples. **h** Comparison of Pyramid and Burrell data

Fig. 8 Ca/Na molar ratio of plagioclase cores, mantles, and rims (bar graphs on y-axis) compared to that of Taranaki glass and rock compositions. Compositions discussed in text (lines with arrows) are projected to show equilibrium melt compositions assuming crystal-melt partition coefficient ($K = 1$). Approximate magma water contents (in wt %) for K are from Martel et al. (2006)



R3 rims record a final zone of declining An, FeO* and MgO contents. The steep An-MgO gradient relative to model curves again indicates a change in melt composition (e.g. Fig. 6c) and is consistent with the resumption of fractional crystallisation. A similar inference for a fractionating melt can be made for the common and significantly wider R1 rims that record an uninterrupted rim-ward trend of declining An, FeO* and MgO contents without reversals in composition (Fig. 6a). Furthermore, these patterns cannot be explained by changes in magmatic $P_{\text{H}_2\text{O}}$ or temperature alone because the depletion of the minor elements requires a change in melt composition.

We also investigated the Fe contents in the phenocrysts. Electron probe data expresses all Fe as FeO* and $\text{Fe}_2\text{O}_3/\text{FeO}$ is unknown. However, the total Fe in plagioclase depends on the melt $\text{Fe}^{3+}/\text{Fe}^{2+}$ (Wilke and Behrens 1999), because the partition coefficient (K) for Fe_2O_3 is significantly higher (~20 times) than that of FeO (Lundgaard and Tegner 2004). Thus, an increase in melt $\text{Fe}_2\text{O}_3/\text{FeO}$ could result in Fe-enriched plagioclase if other factors were constant. In contrast, $K_{\text{Fe}_2\text{O}_3}$ and K_{FeO} are not strongly correlated to plagioclase composition (An) but increase with the silica content of the melt (Lundgaard and Tegner 2004). In natural magmas where Fe is an incompatible element in plagioclase, fractional crystallisation of Fe-Ti oxides will deplete the Fe in the melt producing Fe-poor plagioclase in more evolved melts. This would be recorded as a positive correlation in Fe and Mg profiles in the plagioclase. However, this pattern may not be obvious because by post-crystallisation diffusion of Mg is rapid relative to Fe (Costa et al. 2003).

Most Taranaki phenocrysts show a weak An-FeO* trend in their mantle zones (Fig. 5), but the gradient is variable due to the scatter of FeO* content at similar An content. This is related to compositional changes close to the resorption surfaces. Some resorption and calcic regrowth zones, particularly in oscillatory-zoned phenocrysts (Type 2), are accompanied by invariant FeO* and MgO profiles (Fig. 3a–c), and it is possible that these zones were controlled by changes in $P_{\text{H}_2\text{O}}$ and temperature alone (e.g. Blundy and Cashman 2001; Humphreys et al. 2006). However, in other phenocrysts, resorption surfaces are associated with significant dissolution rounding (Fig. 6a), sieve texture (Fig. 3d), and FeO* (but not MgO) enrichment in the regrowth. R2 rim zones show similar features (Fig. 6b). Such textural characteristics are caused by changes in melt composition (Tsuchiyama 1985; Nakamura and Shimakita 1998). An increase in melt $\text{Fe}^{3+}/\text{Fe}^{2+}$ could promote the partitioning of Fe but not Mg into the plagioclase. Although fractional crystallisation of ferromagnesian phases would preferentially partition Fe^{2+} , this would also deplete the melt of Ca and Mg, inconsistent with the composition of the plagioclase regrowth zones. Depending on the oxidation state of sulphur (S), degassing could also change the oxidation of the melt (see Cottrell

et al. 2022). However, we lack knowledge on the S contents and fluxing for the Taranaki magmas. The preservation of elemental profiles in phenocrysts are dependent on the subsequent thermal history and elemental diffusion rate, i.e. $\text{Mg} > \text{Fe} \geq \text{Ca}$ (Costa et al. 2003). Thus, calcic regrowth zones and R2 rims with elevated Fe and ‘flat’ Mg profiles could be the result of mafic melt recharge and subsequent continuous or pulsed storage at magmatic temperatures of sufficient duration to re-equilibrate the Mg across domain boundaries. We favour this mechanism because of the broad textural similarity of interior resorption/regrowth zones to outermost R3 rims. In addition, the occurrence of R3 rims demonstrates a subsequent thermal disturbance occurred in some phenocrysts.

Taranaki magmatic system and phenocryst origins

Previous workers have inferred a multi-level magma system beneath Taranaki volcano to explain the diversity of rock and mineral compositions (Stewart et al. 1996; Price et al. 1999; Zernack et al. 2012; D’Mello et al. D’Mello et al. 2021, D’Mello et al. 2023). The concept involves a deep magma source in the mantle and/or lower crust and temporary storage at depth where mafic magmas undergo assimilation-fractional crystallisation. Buoyant products then ascend to mid or upper crustal staging zones where magma mixing and further fractional crystallisation occurs. Over time, Taranaki volcano has erupted progressively more K rich magmas (Price et al. 1999), and this is interpreted as increasing crustal contamination of the magmatic system (Zernack et al. 2012). These concepts are broadly the same as the trans-crustal crystal mush system proposed for arc volcanism (e.g., Edmonds et al. 2019; Sparks et al. 2019). The localised high heat flow and shallowing of the seismogenic zone to ~10 km beneath Taranaki volcano (Sherburn and White 2006) could correspond to the top of such a magmatic system.

A conceptual diagram of the Taranaki magma system based on plagioclase characteristics is shown in Fig. 9. In situ $^{87}\text{Sr}/^{86}\text{Sr}$ analyses of plagioclase provide definitive evidence for magma assembly from multiple melt sources. The plagioclase isotopic range ($^{87}\text{Sr}/^{86}\text{Sr} = 0.70440\text{--}0.70486$) is like that of the main edifice lavas (0.70378–0.70504), particularly the post-8 ka rocks (0.7045–0.7050) (Price et al. 1999). However, most samples show inter-crystal disequilibrium where Sr-isotope values for some phenocrysts do not overlap within uncertainty (Fig. 7), indicating some are antecrysts and/or xenocrysts. As isotope disequilibrium is also found for phenocrysts with similar An contents, distinct sources were tapped rather than a lone source that recorded progressive assimilation-fractional crystallisation or various degrees of binary melt mixing. There are also broader inter-eruption differences. For example, plagioclase in the

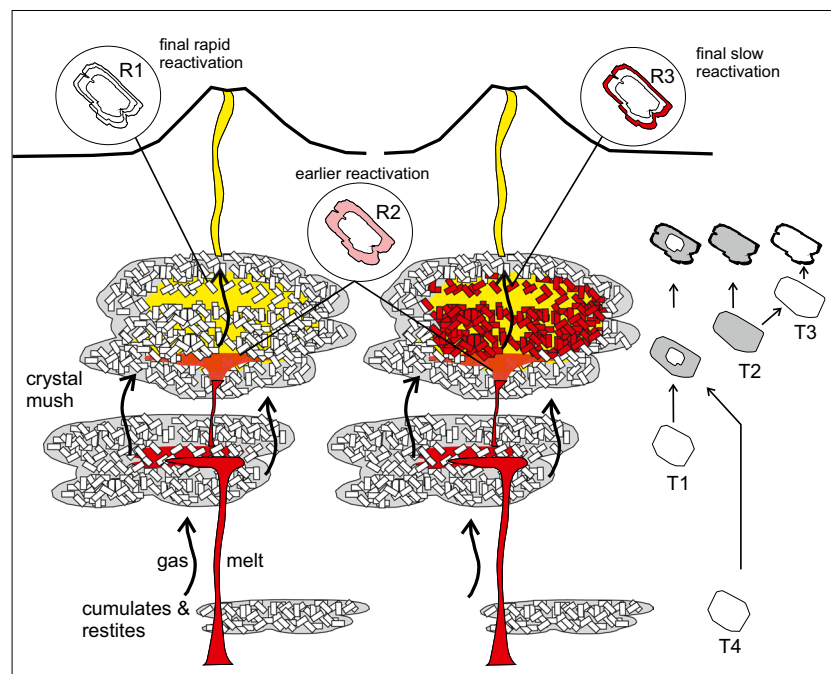


Fig. 9 A conceptual sketch of the magmatic system beneath Taranaki volcano based on a trans-crustal mush system and developed to explain the features of the plagioclase phenocryst cargo. The system is depicted at the time of eruption and melt and gases are transient. Ascending melts, variously decoupled from gas, carry phenocrysts from various sources which then react with their new environments in stages explaining the diversity of textures and isotopic compositions found. Relic cores are entrained from deeper sources and/or earlier

stage crystallisation (T1, 4), while their mantle zones and other phenocrysts (T2) form in staging zones in the upper crust that received inputs of heat, melt and/or gas. Some inputs extensively transform some phenocrysts (T3). If reaction via melts and/or gases of the upper zone is rapid, the rims of the phenocryst do not react to the changes (R1), whereas, if the intrusion or interactions are prolonged, new rims grow (R3). Rim growths from previous intrusions and prolonged heating in other parts of the system can also be erupted (R2)

Pyramid sample on average have higher $^{87}\text{Sr}/^{86}\text{Sr}$ values than those of the Burrell sample across the same compositional (An) range (Fig. 7h). This indicates that the eruptions spaced by 100–200 years (Table 1) tapped a different assemblage of crystals, and those assemblages were inherently heterogeneous. The disruption of crystal mush bodies via thermal and/or fluid influx and buoyant overturn provides an efficient means to transport and mix crystals from different environments (Sparks et al. 2019). If the ascending magma penetrated several mush bodies and/or melt lenses in the conduit, isotopic diversity in the crystal cargo would be expected (Fig. 9).

Most phenocryst populations comprise two or more types in high abundance (>20%), and their relative abundances differ amongst the eruptions (Table 2), further confirming collection from multiple sources. In addition, the phenocrysts grew in dynamic environments. The most common phenocrysts (Type 1) comprise of a relic core ($\sim\text{An}_{70-80}$) and mantle overgrowth ($\sim\text{An}_{50-60}$) that record multiple episodes of resorption and regrowth. These phenocrysts would have been in equilibrium with various andesitic and more calcic (mafic, basalt?) melts during their history (Fig. 8). Most nucleated in a less evolved melt relative to subsequent

growth. If the parental magmas were water under-saturated, decompression during ascent could have increased the water content in the melt causing plagioclase resorption (Blundy and Cashman 2001). Hence, forming the relic skeletal calcic cores. If water saturation in the melt was then reached, subsequent loss of water loss via degassing could have then promoted sodic crystallisation as infill and overgrowth. Other common phenocrysts are characterised by oscillatory-zoned interiors (Type 2). A lack of relic core and their compositions ($\sim\text{An}_{55-65}$) indicate that they represent a later period in magma evolution and nucleated in a melt more silicic than that of the Type 1 phenocrysts (Fig. 8). The oscillatory Ca-Na cycles do not have corresponding changes in Fe or Mg content and likely resulted from fluctuations in T and $P_{\text{H}_2\text{O}}$ in an open system (Blundy and Cashman 2001; Humphreys et al. 2006) or closed-system convective self-mixing (Couch et al. 2001). In addition, both Type 1 and 2 phenocrysts record prominent resorption episodes that caused dissolution rounding of the crystal interiors followed by calcic regrowth. Concurrent changes in MgO and/or FeO^* gradients are best explained by the entry of new magma to the system (see above), in some cases multiple episodes are recorded. Some sodic phenocrysts were so extensively

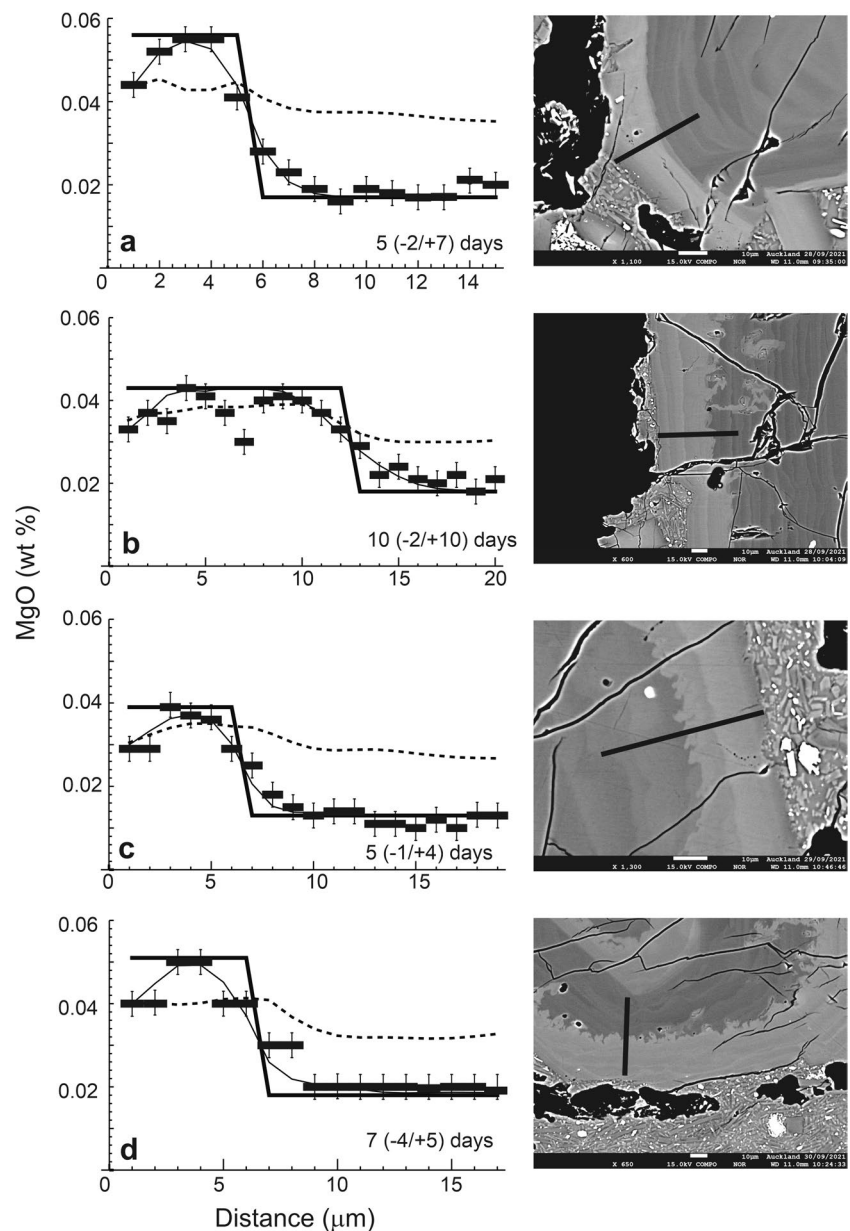
replaced by calcic regrowth that the original texture is not evident (Type 3).

The equilibrium melts for some phenocrysts are beyond the ranges of erupted compositions, such as the calcic ($\text{Ca}/\text{Na} > 5$; $> \text{An}_{83}$) relic cores in Type 4 phenocrysts (Fig. 8). Similar crystal compositions are found in some gabbro and ultramafic xenoliths erupted at Taranaki volcano, as noted by D'Mello et al. (2023). Thus, Type 4 relic cores must have been entrained into their host magma and could result from xenolith disintegration. The xenoliths in Taranaki rocks are thought to be derived from deep cumulates, cognate to their host rocks due to their geochemical and isotopic affinity; while others may be restites associated with crustal anatexis (Price et al. 2016).

Timescales recorded in phenocryst rims

We estimated the duration of crystal rim formation to eruption through modelling the diffusive re-equilibration of Mg using plagioclase phenocrysts with a simple reverse-zoned rim overgrowth (R3 rims) and sharp elemental gradients at the resorption surface (see 'Methods' section). Our estimates are only an approximation because of the assumed temperature and the analytical spatial resolution on the short compositional gradients, both of which have a significant impact on modelling. We report mainly the results of using a temperature of 950 °C (see above) but also explored the effects a temperature range of 900 to 1000 °C. Diffusion modelling was attempted for 26 phenocrysts (Fig. 10; Online Resource

Fig. 10 Examples of diffusion models for plagioclase phenocrysts. **a, b** Pyramid (67411A-03; 67411B-03). **c** Newall (M1H-A08). **d** Te Popo (P1A-A17). The initial condition (thick line) is based on the An content at the analytical spots for observed MgO content (black uncertainty bars). MgO equilibrium values (dashed line) are calculated by K_{Mg} (Mutch et al. 2022) and a temperature of 950 °C. Results for the diffusion model are shown with a thin black line. The estimated time for an initial step function in MgO to decay to the observed data is shown. Black line on BSE image shows position of analytical profile



1). Using the K_{Mg} of Mutch et al. (2022), 14 had no observable Mg diffusive redistribution relative to Ca-Na, i.e. the core-overgrowth transition had the same width, at the analytical resolution used (3-mm-diameter electron beam spots with a 3-mm spacing). This implies a maximum time elapsed of <1 day between regrowth and quenching for the model conditions mentioned above. In addition, four phenocrysts produced model fits for durations of ~5–10 days with uncertainty of similar magnitude (Fig. 10). The remainder of the phenocrysts are not suitable for modelling due to their more complex multi-stage growth histories like that observed at other volcanoes (Didonna et al. 2022). At 900 °C and 1000 °C, the time estimates would change by a factor of ~3 (increase) and 0.5 (decrease), respectively. These estimates do not include the period associated with resorption or the total residence time in the crust. Although the equilibrium profiles calculated with the Mutch et al. (2022) and Bindeman et al. (1998) formulations are quite different, due to the short gradients and thus limited equilibration of Mg, the times calculated with both formulations are within error (Online Resource 1). Higgins (1996) interpreted plagioclase crystal size distributions in Taranaki rocks as formation in constant conditions such as single-event cooling over periods of ~30–75 years. Such time estimates would represent the entire crystal growth rather than the final rim examined here. However, isotopic and textural diversity demonstrates that some phenocrysts of comparable size are not part of a genetically related population. Thus, a single-event cooling history is unlikely.

Magma recharge and eruption triggers

A temporal trend to less evolved rock compositions during the eruptions of ~1130 to 1800 CE has been interpreted as new magma entering the system and initially re-activating older evolved magma (Lerner et al. 2019). The Ca- and Fe- rich resorption/regrowth zones in the interiors of the plagioclase phenocrysts suggest that multiple melt injection events occurred in all magmas studied. Their flat Mg profiles indicate subsequent re-equilibration via storage in a warm magma. Thus, the priming to eruption was a multi-stage process. However, the final magmatic conditions just before eruption differed in some events. Approximately 80–90% of phenocrysts in the Te Popo, Newall and Pyramid samples have R3 rims with steep An, Fe and Mg profiles (Table 2) that record regrowth in a more mafic melt, consistent with new magma injection within a few days of eruption (see above). Comparable short timescales have been determined for plagioclase with similar textural features in andesites from Mt Hood and Soufrière Hills volcanoes where mafic magma influx is inferred as an eruption trigger (Didonna et al. 2022; Kent et al. 2010).

In contrast, >90% of phenocrysts in the Burrell sample (and pre-1 ka Summit and Staircase samples) have R1 rims and those in the Tahurangi sample (and the pre-1 ka Warwick's Castle sample) have a mixture of R1 and R2 rims (Table 2). R1 rims record uninterrupted growth consistent with increasing crystallinity of the magma. While R2 rims likely resulted from an earlier episode of mafic influx followed by further magmatic storage. There are examples of eruptions where the phenocrysts lack evidence for final magmatic recharge and an internal trigger has been proposed. These include magma pressurisation from crystallisation-induced exsolution of volatiles in the 2014 Kelud and 2015 Calbuco eruptions (Arzilli et al. 2019; Cassidy et al. 2019); or open-system volatile 'flushing' of the conduit from deeper degassing for the 1990 Kelud eruption (Utami et al. 2021).

However, the reactivation of crystal mush bodies via intrusion can be incremental and only involve small areas of the system such as the floor, until thermal/buoyancy instability produces complete collapse and remobilisation (Bergantz et al. 2017; Schleicher and Bergantz 2017). As a result, some crystals may experience multiple changes in magmatic environment while others may not. Fluid dynamic modelling indicates that the formation of reaction rims on crystals and the magnitude of their elemental gradients are a function of proximity to the intrusion and the duration of the intrusion before eruption (Cheng et al. 2020). This can explain why some phenocryst populations record different timescales within the same rock, such as those erupted at La Soufrière de Guadeloupe (Metcalf et al. 2021).

Thus, the rate of mush reactivation may have dictated the mineralogical response in Taranaki magmas (Fig. 9). In this scenario, phenocrysts in the Te Popo, Newall and Pyramid magmas had sufficient time to react to melt mixing (R3 rims). In contrast, mush reactivation in the Burrell eruption may have been sufficiently rapid that most phenocrysts did not record the event (R1 rims). The contrasting histories of rapid reactivation (R1 rims) and prolonged heating following recharge (R2 rims) in the Tahurangi magma, and the occurrence of subordinate rim types in other magmas, may reflect phenocryst collection from melt lenses that had different thermal regimes, as proposed for La Soufrière de Guadeloupe magmas (Metcalf et al. 2021). Pre-eruption intrusion durations of up to decades and intrusion hiatus of ~1 year preceding some events at Popocatepetl volcano have been inferred from clinopyroxene diffusion chronometry (Mangler et al. 2022). Thus, it is possible that elements with high diffusion rates such as Mg in plagioclase only record the final days or weeks of a potentially longer and discontinuous intrusive history.

If the rate of crystal mush reactivation was the main control on the phenocryst textures, then why did the rates vary? Each of the post-1 ka Taranaki eruptions studied had similar magnitudes (Lerner et al. 2019), and thus, similar

eruptible magma volumes. Also, their eruption styles were broadly similar involving explosive ash emission and lava dome extrusion. The minor differences in their whole-rock compositions (Table 1) do not provide compelling evidence for differing degrees of mixing with new mafic melt that could have influenced remobilisation. It has long been proposed that the migration and accumulation of hot volatiles is required for disruption and eruption of a crystal mush (e.g. Bachmann and Bergantz 2006; Ruprecht et al. 2008; Edmonds et al. 2019). Furthermore, the recharge process may involve significant melt/gas decoupling leading to separate migration and storage in the crust during quiescence or unrest. Thus, contributing to instabilities in the magmatic system (Christopher et al. 2015; Caricchi et al. 2018). Not surprisingly, the total volatile budget and nature of degassing of unerupted magmas could be a key in understanding unrest at Taranaki volcano.

Concluding remarks

Every mineral type provides a different view into magma genesis as each variously records only parts of the history depending on their time of formation and rate of reaction to environmental changes. In the case of Taranaki volcano, in situ Sr-isotope analysis of plagioclase phenocrysts provides definitive evidence for disequilibrium and assembly from multiple melt lenses or incrementally grown mush bodies, and subordinately from the disintegration of xenoliths entrained from deeper cumulates or restites. Thus, many phenocrysts are antecrystic and/or xenocrystic. Consecutive eruptions spaced by ~100 or 200 years have extracted isotopically different phenocryst populations indicating the magma reservoirs changed or formed rapidly. Crystal dissolution/regrowth textures and elemental zonation coupled with the relative rates of post-crystallisation elemental diffusion ($Mg > Fe > Ca$) were used to infer the entry of new mafic melt into each magma batch. Many phenocryst interiors record several such episodes and subsequent storage at elevated temperature. Thus, eruption priming was multi-stage. However, the final rim overgrowths on the phenocrysts are distinct in some eruptions. Continuous rim growth consistent with fractional crystallisation of a cooling magma is recorded in some eruptions. In others, rim regrowth following partial dissolution records the input of new mafic melt occurred just days before eruption (based on Mg chronometry). This raises a question in interpreting eruption triggers from distinct mineral textures: either the triggering mechanism differed (internal versus external) or the rate of reservoir remobilisation dictated whether a mineralogical response occurred.

Supplementary Information The online version contains supplementary material available at <https://doi.org/10.1007/s00445-023-01661-0>.

Acknowledgements David Neave and an anonymous reviewer are thanked for their comments on the manuscript. Martin Mangler and Olivier Reubi provided valuable insight on an earlier version. We thank David Adams for assistance with electron microprobe operation.

Funding Open Access funding enabled and organized by CAUL and its Member Institutions This study was supported by the Ministry for Business, Innovation and Employment Endeavour Fund Contract UOAX1913. PS also acknowledges the University of Auckland Faculty Development Research Fund.

Open Access This article is licensed under a Creative Commons Attribution 4.0 International License, which permits use, sharing, adaptation, distribution and reproduction in any medium or format, as long as you give appropriate credit to the original author(s) and the source, provide a link to the Creative Commons licence, and indicate if changes were made. The images or other third party material in this article are included in the article's Creative Commons licence, unless indicated otherwise in a credit line to the material. If material is not included in the article's Creative Commons licence and your intended use is not permitted by statutory regulation or exceeds the permitted use, you will need to obtain permission directly from the copyright holder. To view a copy of this licence, visit <http://creativecommons.org/licenses/by/4.0/>.

References

- Arzilli F, Morgavi D, Petrelli M, Polacci M, Burton M, Di Genova D et al (2019) The unexpected explosive sub-Plinian eruption of Calbuco volcano (22–23 April 2015; southern Chile): triggering mechanism implications. *J Volcan Geotherm Res* 378:35–50. <https://doi.org/10.1016/j.jvolgeores.2019.04.006>
- Bachmann O, Bergantz GW (2006) Gas percolation in upper-crustal silicic crystal mushes as a mechanism for upward heat advection and rejuvenation of near-solidus magma bodies. *J Volcan Geotherm Res* 149:85–102
- Bergantz GW, Schleicher JM, Burgisser A (2017) On the kinematics and dynamics of crystal-rich systems. *J Geophys Res: Solid Earth* 122(8):6131–6159
- Bindeman IN, Davis AM, Drake MJ (1998) Ion microprobe study of plagioclase-basalt partition experiments at natural concentration levels of trace elements. *Geochim Cosmochim Acta* 62:1175–1193
- Blundy J, Cashman K (2001) Ascent-driven crystallisation of dacite magmas at Mount St. Helens, 1980–1986. *Contrib Mineral Petrol* 140:631–650
- Caricchi L, Sheldrake TE, Blundy J (2018) Modulation of magmatic processes by CO₂ flushing. *Earth Planet Sci Lett* 491:160–171. <https://doi.org/10.1016/j.epsl.2018.03.042>
- Cassidy M, Ebmeier SK, Helo C, Watt SFL, Caudron C, Odell A et al (2019) Explosive eruptions with little warning: experimental petrology and volcano monitoring observations from the 2014 eruption of Kelud, Indonesia. *Geochem Geophys Geosyst* 20:4218–4247. <https://doi.org/10.1029/2018gc008161>
- Cheng L, Costa F, Bergantz G (2020) Linking fluid dynamics and olivine crystal scale zoning during simulated magma intrusion. *Contrib Mineral Petrol* 175:53. <https://doi.org/10.1007/s00410-020-01691-3>
- Cherniak DJ (2010) Cation diffusion in feldspars. *Rev Mineral Geochem* 72:691–733. <https://doi.org/10.2138/rmg.2010.72.15>

- Christopher TE, Blundy J, Cashman K, Cole P, Edmonds M, Smith PJ, Sparks RSJ, Stinton A (2015) Crustal-scale degassing due to magma system destabilization and magma-gas decoupling at Soufrière Hills Volcano, Montserrat. *Geochem Geophys Geosyst* 16:2797–2811. <https://doi.org/10.1002/2015GC005791>
- Cocker K, Shane P, Cronin S, Stirling C, Reid M (2022) A history of andesite production via magma mixing and mingling revealed microscopically at Ngauruhoe volcano. *Geochem Geophys Geosyst* 23:e2022GC010589. <https://doi.org/10.1029/2022GC010589>
- Cocker K, Shane P, Stirling C, Reid M (2021) Constraints on assembly of Tongariro and Ruapehu andesite magmas based on Sr-isotope compositions of plagioclase and groundmass. *Lithos* 400–401:106406. <https://doi.org/10.1016/j.lithos.2021.106406>
- Cole JW (1990) Structural control and origin of volcanism in the Taupo Volcanic Zone, New Zealand. *Bull Volcanol* 52:445–459
- Coombs ML, Sisson TW, Bleick HA, Henton SM, Nye CJ, Payne AL et al (2013) Andesites of the 2009 eruption of Redoubt Volcano, Alaska. *J Volcanol Geotherm Res* 259:349–372. <https://doi.org/10.1016/j.jvolgeores.2012.01.002>
- Costa F (2021) Clocks in magmatic rocks. *Ann Rev Earth Planet Sci* 49:231–252. <https://doi.org/10.1146/annurev-earth-080320-060708>
- Costa F, Chakraborty S (2004) Decadal time gaps between mafic intrusion and silicic eruption obtained from chemical zoning patterns in olivine. *Earth Planet Sci Lett* 227:517–530
- Costa F, Chakraborty S, Dohmen R (2003) Diffusion coupling between trace and major elements and a model for calculation of magma residence times using plagioclase. *Geochim Cosmochim Acta* 67:2189–2200
- Cottrell E, Birner SK, Brounce M, Davis FA, Waters LE, Kelley KA (2022) Oxygen fugacity across tectonic settings. In: Moretti R, Neuville RD (eds) *Magma Redox Geochemistry*. Geophysical Monograph Series. American Geophysical Union, pp 33–61. <https://doi.org/10.1002/9781119473206.ch3>
- Couch S, Sparks RSJ, Carroll MR (2001) Mineral disequilibrium in lava explained by convective self-mixing in open magma chambers. *Nature* 411:1037–1039
- Cronin SJ, Zernack AV, Ukstins IA, Turner MB, Torres-Orozco R, Stewart RB et al (2021) The geological history and hazards of a long-lived stratovolcano, Mt. Taranaki, New Zealand. *NZ J Geology Geophys* 64:456–478. <https://doi.org/10.1080/00288306.2021.1895231>
- D’Mello NG, Zellmer GF, Kereszturi G, Ubide T, Procter JN, Stewart RB (2023) Crystal entrainment from cool, low-silica rocks into hot, high-silica melts: diverse primary melt compositions at Taranaki volcano, New Zealand. *J Geol Soc* 180. <https://doi.org/10.1144/jgs2022-036>
- Damaschke M, Cronin SJ, Bebbington MS (2018) A volcanic event forecasting model for multiple tephra records, demonstrated on Mt. Taranaki, New Zealand. *Bull Volcanol* 80:9. <https://doi.org/10.1007/s00445-017-1184-y>
- Damaschke M, Cronin SJ, Torres-Orozco R, Wallace RC (2017) Unifying tephrostratigraphic approaches to redefine major Holocene marker tephra, Mt Taranaki, New Zealand. *J Volcanol Geotherm Res* 337:29–43
- Davidson JP, Morgan DJ, Charlier BL, et. al. (2007) Microsampling and isotopic analysis of igneous rocks: implications for the study of magmatic systems. *Ann Rev Earth Planet Sci* 35:273–311.
- Didonna R, Costa F, Handley H, Turner S, Barclay J (2022) Dynamics and timescales of mafic–silicic magma interactions at Soufrière Hills Volcano, Montserrat. *Cont Mineral Petrol* 177:28. <https://doi.org/10.1007/s00410-022-01891-z>
- D’Mello NG, Zellmer GF, Negrini M, Kereszturi G, Procter J, Stewart R et al (2021) Deciphering magma storage and ascent processes of Taranaki, New Zealand, from the complexity of amphibole breakdown textures. *Lithos* 398–399:106264. <https://doi.org/10.1016/j.lithos.2021.106264>
- Edmonds M, Cashman KV, Holness M, Jackson M (2019) Architecture and dynamics of magma reservoirs. *Philos Trans R Soc A* 377:20180298. <https://doi.org/10.1098/rsta.2018.0298>
- Ginibre C, Wörner G, Kronz A (2002) Minor- and trace-element zoning in plagioclase: implications for magma chamber processes at Parícuta volcano, northern Chile. *Cont Mineral Petrol* 143:300–315
- Ginibre C, Worner G, Kronz A (2007) Crystal zoning as an archive for magma evolution. *Elements* 3:261–266
- Girona T, Costa F, Schubert G (2016) Degassing during quiescence as a trigger of magma ascent and volcanic eruptions. *Sci Rep* 5:18212. <https://doi.org/10.1038/srep18212>
- Grove TL, Baker MB, Kinzler RJ (1984) Coupled CaAl–NaSi diffusion in plagioclase feldspar: experiments and applications to cooling rate speedometry. *Geochim Cosmochim Acta* 48:2113–2121
- Higgins MD (1996) Crystal size distributions and other quantitative textural measurements in lavas and tuff from Egmont volcano (Mt. Taranaki), New Zealand. *Bull Volcanol* 58:194–204
- Humphreys MCS, Blundy JD, Sparks RSJ (2006) Magma evolution and open-system processes at Shiveluch Volcano: insights from phenocryst zoning. *J Petrol* 47:2303–2334
- Kent AJR, Darr C, Koleszar AM, Salisbury MJ, Cooper KM (2010) Preferential eruption of andesitic magmas through recharge filtering. *Nat Geosci* 3:631–636. <https://doi.org/10.1038/Ngeo924>
- Lerner G, Cronin SJ, Bebbington MS, Platz T (2019) The characteristics of a multi-episode volcanic regime: the post-AD960 Maero Eruptive Period of Mt. Taranaki (New Zealand). *Bull Volcanol* 81:61. <https://doi.org/10.1007/s00445-019-1327-4>
- Lundgaard KL, Tegner C (2004) Partitioning of ferric and ferrous iron between plagioclase and silicate melt. *Cont Mineral Petrol* 147:470–483
- Mangler MF, Petrone CM, Prytulak J (2022) Magma recharge patterns control eruption styles and magnitudes at Popocatepetl volcano (Mexico). *Geology* 50:366–370. <https://doi.org/10.1130/G49365.1>
- Martel C, Pichavant M, Holtz F, Scaillet B, Bourdier JL, Traîneau H (1999) Effects of fO₂ and H₂O on andesite phase relations between 2 and 4 kbar. *J Geophys Res* 104:29453–29470
- Martel C, Radadi Ali A, Poussineau S, Gourgaud A, Pichavant M (2006) Basalt-inherited microlites in silicic magmas: evidence from Mount Pelée (Martinique, French West Indies). *Geology* 34:905–908. <https://doi.org/10.1130/G22672A.1>
- Metcalfe A, Moune S, Komorowski J-C et al (2021) Magmatic processes at La Soufrière de Guadeloupe: Insights from crystal studies and diffusion timescales for eruption onset. *Front. Earth Sci* 9:617294. <https://doi.org/10.3389/feart.2021.617294>
- Molloy C, Shane P, Augustinus P (2009) Eruption recurrence rates in a basaltic volcanic field based on tephra layers in maar sediments: implications for hazards in the Auckland Volcanic Field. *Geol Soc Am Bull* 12:1666–1677. <https://doi.org/10.1130/B26447.1>
- Murphy MD, Sparks RSJ, Barclay J, Carroll MR, Brewer TS (2000) Remobilization of andesite magma by intrusion of mafic magma at the Soufrière Hills Volcano, Montserrat, West Indies. *J Petrol* 41:21–42. <https://doi.org/10.1093/petrology/41.1.21>
- Mutch EJF, MacLennan J, Madden-Nadeau AL (2022) The dichotomous nature of Mg partitioning between plagioclase and melt: Implications for diffusion chronometry. *Geochim Cosmochim Acta* 339:173–189. <https://doi.org/10.1016/j.gca.2022.10.035>
- Nakamura M, Shimakita S (1998) Dissolution origin and syn-entrapment compositional change of melt inclusion in plagioclase. *Earth Planet Sci Lett* 161:119–133
- Pallister J, McNutt SR (2015) Synthesis of volcano monitoring. In: Sigurdsson H, Houghton B, McNutt SR, Rymer H, Stix J (eds) *The Encyclopedia of Volcanoes*, 2nd edn. Elsevier, Amsterdam, pp 1151–1171. <https://doi.org/10.1016/B978-0-12-385938-9.00066-3>

- Pallister JS, Hoblitt RP, Meeker GP, Knight RJ, Siems DF (1996) Magma mixing at Mount Pinatubo; petrographic and chemical evidence from the 1991 deposits. In: Newhall CG, Punongbayan R (eds) *Fire and Mud. Eruptions and Lahars of Mount Pinatubo, Philippines*, University of Washington Press, Seattle, pp 687–732
- Panjasawatwong Y, Danyushevsky LV, Crawford AJ, Harris KL (1995) An experimental study of the effects of melt composition on plagioclase—melt equilibria at 5 and 10 kbar: implications for the origin of magmatic high-An plagioclase. *Cont Mineral Petrol* 118:420–432
- Platz T, Cronin SJ, Cashman KV, Stewart RB, Smith IEM (2007) Transitions from effusive to explosive phases in andesite eruptions – a case-study from the AD1655 eruption of Mt. Taranaki. *New Zealand. J Volcanol Geotherm Res* 161:15–34
- Platz T, Cronin SJ, Procter JN, Neall VE, Foley S (2012) Nonexplosive, dome-forming eruptions at Mt. Taranaki, New Zealand. *Geomorphol* 136:15–30
- Price RC, Smith IEM, Stewart RB, Gamble JA, Gruender K, Maas R (2016) High-K andesite petrogenesis and crustal evolution: Evidence from mafic and ultramafic xenoliths, Egmont Volcano (Mt. Taranaki) and comparisons with Ruapehu Volcano, North Island, New Zealand. *Geochim Cosmochim Acta* 185:328–357
- Price RC, Stewart RB, Woodhead JD, Smith IEM (1999) Petrogenesis of high-K arc magmas: evidence from Egmont Volcano, North Island, New Zealand. *J Petrol* 40:167–197
- Reyners M, Eberhart-Phillips D, Stewart G, Nishimura Y (2006) Imaging subduction from the trench to 300 km depth beneath the central North Island, New Zealand, with Vp and Vp/Vs. *Geophys J Int* 165:565–583
- Ruprecht P, Bergantz GW, Dufek J (2008) Modeling of gas-driven magmatic overturn: tracking of phenocryst dispersal and gathering during magma mixing. *Geochem Geophys Geosyst* 9:Q07017. <https://doi.org/10.1029/2008GC002022>
- Schleicher JM, Bergantz GW (2017) The mechanics and temporal evolution of an open-system magmatic intrusion into a crystal-rich magma. *J Petrol* 58:1059–1072. <https://doi.org/10.1093/ptrology/egx045>
- Shane P, Cocker K, Coote A, Stirling CH, Reid MR (2019) The prevalence of plagioclase antecrysts and xenocrysts in andesite magma, exemplified by lavas of the Tongariro volcanic complex, New Zealand. *Cont Mineral Petrol* 174:89. <https://doi.org/10.1007/s00410-019-1626-y>
- Sherburn S, White RS (2006) Tectonics of the Taranaki region, New Zealand: earthquake focal mechanisms and stress axes. *NZ J Geol Geophys* 49:269–279
- Singer BS, Dungan MA, Layne GD (1995) Textures and Sr, Ba, Mg, Fe, K, and Ti compositional profiles in volcanic plagioclase: clues to the dynamics of calc-alkaline magma chambers. *Am Mineral* 80:776–798
- Sisson TW, Grove TL (1993) Experimental investigations of the role of H₂O in calc-alkaline differentiation and subduction zone magmatism. *Cont Mineral Petrol* 113:143–166. <https://doi.org/10.1007/BF00283225>
- Smith VC, Blundy JD, Arce JL (2009) A temporal record of magma accumulation and evolution beneath Nevado de Toluca, Mexico, preserved in plagioclase phenocrysts. *J Petrol* 50:405–426. <https://doi.org/10.1093/ptrology/egp005>
- Sparks RSJ, Annen C, Blundy JD, Cashman KV, Rust AC, Jackson MD (2019) Formation and dynamics of magma reservoirs. *Philos Trans R Soc A*. 377:20180019. <https://doi.org/10.1098/rsta.2018.0019>
- Stewart RB, Price RC, Smith IEM (1996) Evolution of high-K arc magma, Egmont volcano, Taranaki, New Zealand: evidence from mineral chemistry. *J Volcanol Geotherm Res* 74:275–295
- Tait S, Jaupart C, Vergnolle S (1989) Pressure, gas content and eruption periodicity of a shallow, crystallising magma chamber. *Earth Planet Sci Lett* 92:107–123. [https://doi.org/10.1016/0012-821X\(89\)90025-3](https://doi.org/10.1016/0012-821X(89)90025-3)
- Tsuyuhama A (1985) Dissolution kinetics of plagioclase in the melt of the system diopside–albite–anorthite, and origin of dusty plagioclase in andesites. *Cont Mineral Petrol* 89:1–16
- Ubide T, Kamber BS (2018) Volcanic crystals as time capsules of eruption history. *Nat Commun* 9:326. <https://doi.org/10.1038/s41467-017-02274-w>
- Utami SB, Costa F, Lesage PH, Allard P, Humaida H (2021) Fluid fluxing and accumulation drive decadal and short-lived explosive basaltic andesite eruptions preceded by limited volcanic unrest. *J Petrol* 62:1–29. <https://doi.org/10.1093/ptrology/egab086>
- Van Orman JA, Cherniak DJ, Kita NT (2014) Magnesium diffusion in plagioclase: dependence on composition, and implications for thermal resetting of the Al-26-Mg-26 early solar system chronometer. *Earth Planet Sci Lett* 385:79–88. <https://doi.org/10.1016/j.epsl.2013.10.026>
- Wilke M, Behrens H (1999) The dependence of the partitioning of iron and europium between plagioclase and hydrous tonalitic melt and oxygen fugacity. *Cont Mineral Petrol* 137:102–114
- Zernack AV, Price RC, Smith IEM, Cronin SJ, Stewart RB (2012) Temporal evolution of a high-K andesitic magmatic system: Taranaki Volcano, New Zealand. *J Petrol* 53:325–363
- Zorn E (2017) Geochemistry and groundmass crystallinity controls on lava dome stability at Mount Taranaki, New Zealand. Dissertation, University of Auckland